Research

A model of bidirectional synaptic plasticity: From signaling network to channel conductance

Gastone C. Castellani,[1,2,6] Elizabeth M. Quinlan,[4] Ferdinando Bersani,[1] Leon N. Cooper,[2,3] and Harel Z. Shouval[2,5]

[1]*Physics Department, DIMORFIPA, CIG, Bologna University, Bologna 40137, Italy;* [2]*Institute for Brain and Neural Systems and* [3]*Physics and Neuroscience Department, Brown University, Providence, Rhode Island 02912, USA;* [4]*Neuroscience and Cognitive Sciences Program, University of Maryland, College Park, Maryland 20742, USA;* [5]*Department of Neurobiology and Anatomy, University of Texas Medical School at Houston, Houston, Texas 77030, USA*

In many regions of the brain, including the mammalian cortex, the strength of synaptic transmission can be bidirectionally regulated by cortical activity (synaptic plasticity). One line of evidence indicates that long-term synaptic potentiation (LTP) and long-term synaptic depression (LTD), correlate with the phosphorylation/dephosphorylation of sites on the α-Amino-3-hydroxy-5-methyl-4-isoxazolepropionic acid (AMPA) receptor subunit protein GluRI. Bidirectional synaptic plasticity can be induced by different frequencies of presynaptic stimulation, but there is considerable evidence indicating that the key variable is calcium influx through postsynaptic *N*-methyl-D-aspartate (NMDA) receptors. Here, we present a biophysical model of bidirectional synaptic plasticity based on [Ca^{2+}]-dependent phospho/dephosphorylation of the GluRI subunit of the AMPA receptor. The primary assumption of the model, for which there is wide experimental support, is that the postsynaptic calcium concentration, and consequent activation of calcium-dependent protein kinases and phosphatases, is the trigger for phosphorylation/dephosphorylation at GluRI and consequent induction of LTP/LTD. We explore several different mathematical approaches, all of them based on mass-action assumptions. First, we use a first order approach, in which transition rates are functions of an activator, in this case calcium. Second, we adopt the Michaelis-Menten approach with different assumptions about the signal transduction cascades, ranging from abstract to more detailed and biologically plausible models. Despite the different assumptions made in each model, in each case, LTD is induced by a moderate increase in postsynaptic calcium and LTP is induced by high Ca^{2+} concentration.

The majority of fast excitatory synaptic transmission in the mammalian central nervous system is mediated by the AMPA (α-Amino-3-hydroxy-5-methyl-4-isoxazolepropionic acid) subtype of ionotropic glutamate receptor. As such, changes in the conductance of individual AMPA receptors (AMPARs) will have a significant effect on the efficacy of synaptic transmission. Phosphorylation and dephosphorylation of receptors have been shown to be major mechanisms of regulation of synaptic strength (Walaas and Greengard 1991; Malinow and Malenka 2002). The signal-transduction cascades controlling synaptic phosphorylation/dephosphorylation are complex, and mathematical descriptions of such networks are essential in order to obtain a quantitative understanding of their function. AMPA receptors are tetramers composed of four homologous subunit proteins (GluR1–GluR4) that combine to form different AMPA receptor subtypes (Petralia and Wenthold 1992). The AMPA receptor subunit protein GluR1 is one of the most abundantly expressed subunits in the mammalian hippocampus and neocortex, and in combination with GluR2, is thought to comprise the majority of AMPA receptor complexes in these regions (Wenthold et al. 1996). Several serine residues in the intracellular carboxy-terminal tail of GluR1 have been identified as important sites for activity-dependent regulation of AMPA receptor function by phosphorylation. Protein kinase A (PKA) specifically phosphorylates serine 845 (S845), while protein kinase C (PKC) and CaMKII phosphorylate serine 831 (S831). Phosphorylation of S831 increases the unitary conductance of the AMPAR, and phosphorylation at S845 increases the channel mean open time, in both cases increasing the average channel conductance (Roche et al. 1996; Barria et al. 1997; Benke et al. 1998; Derkach et al. 1999; Banke et al. 2000). Dephosphorylation at each site is mediated by an activity-dependent protein phosphatase cascade. Long term potentiation (LTP), a sustained increase in synaptic strength, is associated with an increased phosphorylation at S831 (Barria et al. 1997; Lee et al. 2000a), whereas long term depression (LTD), a sustained decrease in synaptic strength, has been associated with a decrease in S845 phosphorylation (Kameyama et al. 1998; Lee et al. 1998, 2000a).

A considerable body of evidence indicates that a key variable controlling the sign and magnitude of synaptic plasticity is the amount of integrated postsynaptic NMDA receptor (NMDAR) activation (Dudek and Bear 1992; Mulkey and Malenka 1992; Cummings et al. 1996). Modest NMDAR activation, induced by low-frequency stimulation, results in LTD, while strong, high-frequency activation produces LTP. NMDAR's are permeable to Ca^{2+}; therefore, it has been proposed that an increase in postsynaptic calcium is a primary signal for the induction of bidirectional synaptic plasticity (Bear et al. 1987; Lisman 1989; Artola and Singer 1993). A robust, transient increase in postsynaptic calcium is observed during high-frequency stimulation (HFS), while a modest prolonged increase in postsynaptic calcium is observed during low-frequency stimulation (LFS). Indeed, chelating postsynaptic calcium with EGTA blocks both high-frequency-induced LTP and low-frequency-induced LTD (Lynch et al. 1983; Brocher et al. 1992). Here, we present a model of bidirectional synaptic plasticity (Fig. 1) based on regulation of AMPAR func-

[6]Corresponding author.
E-mail gasto@alma.unibo.it; fax 39-051-2097899.
Article published online ahead of print. Article and publication date are at http://www.learnmem.org/cgi/doi/10.1101/lm.80705.

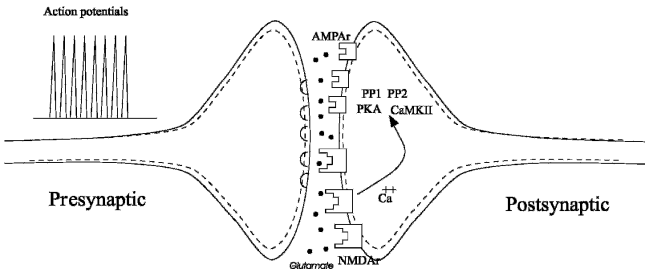

Figure 1. A schematic of an excitatory glutamatergic synapse. Action potentials traveling down the presynaptic axon trigger the calcium-dependent release of glutamate. Glutamate binds to two types of postsynaptic ionotropic receptors, NMDARs and AMPARs. The postsynaptic terminal contains a set of enzymes (PP1, PP2b, PKA, CaMKII) that transduce the influx of Ca^{2+} through the NMDARs into changes in the phosphorylation state of GluR1, thereby regulating AMPAR conductance.

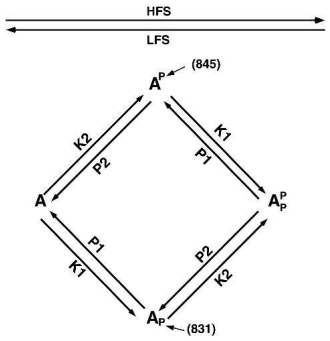

Figure 2. General model of the phosphorylation/dephosphorylation cycle of the GluR1 subunit of the AMPAR. There are two phosphorylation sites on the GluR1 subunit of the AMPAR, serine 845 (S845) and Serine 831 (S831). GluR1 can be dephosphorylated at both sites (*A*), phosphorylated at S845 (A^{p2}), phosphorylated at S831 (A_{p1}), or phosphorylated at both S845 and S831 (A_{p1}^{p2}). We assume two pairs of enzymes, the enzyme kinase 1 (K1)/enzyme phosphatase 1 (P1) pair phosphorylate and dephosphorylate site 1 (S831), whereas the enzyme kinase 2 (K2)/enzyme phosphatase 2 (P2) pair phosphorylate and dephosporylate site 2 (S845). High-frequency stimulation of the synapses (HFS) activates protein kinases, resulting in phosphorylation. Low-frequency stimulation of the synapse (LFS) activates protein phosphatases, resulting in phosphorylation.

tion by a $[Ca^{2+}]$-dependent phosphorylation/dephosphorylation of GluR1. Throughout this work, we adopt a general set of assumptions that calcium is the primary signal regulating bidirectional synaptic plasticity through the differential activation of protein kinases and phosphatases (Lisman 1989). We use several different mathematical approaches to analyze the AMPAR phosphorylation at different calcium levels with increasing mathematical complexity and biological realism. Our results indicate that a small rise in postsynaptic calcium results in AMPAR dephosphorylation, while a larger rise produces phosphorylation of AMPARs. These results are qualitatively robust, and do not depend on the type of mathematical analysis used. We develop mathematical formalisms for analysis of synaptic plasticity through the phosphorylation of AMPA receptors at two different sites (see below).

As shown below, we model a subnetwork of enzymes that links calcium level to AMPAR phosphorylation. This detailed model of the signal-transduction cascade examines the validity of the more abstract assumptions made in previous sections. Synaptic strength is directly related to AMPAR receptor conductance, the number of postsynaptic receptors, and the presynaptic probability of neurotransmitter release. In this work, we focus on changes in AMPAR conductance via phosphorylation, and therefore, use the terms phosphorylation state, receptor conductance, and synaptic strength interchangeably.

This study is an extension of previous work (Castellani et al. 2001), in which we developed a model of bidirectional synaptic plasticity using a first order Mass Action approach. Here, we analyze a more detailed model using a more precise mathematical formalism and a specific, experimentally motivated signal-transduction cascade leading from the rise in calcium levels to changes in enzymatic activity.

The AMPAR phosphorylation cycle

A model for the AMPAR phosphorylation cycle

A first step toward the construction of a model for the AMPAR phosphorylation cycle (Fig. 2) is to note that the involved kinases and phosphatases can be grouped in phospho–dephospho couples acting on the same substrate. We will refer to these enzymes as K1, P1, K2, and P2, where K1 stands for Enzyme Kinase of type 1, P1 for Enzyme Phosphatase of type 1, and so on. These enzymes act on the GluR1 subunit (*A*) that can be phosphorylated and dephosphorylated at different sites, with high specificity. We make a crucial assumption, supported by sufficient experimental evidence (Meyer et al. 1992), that these enzymes are differentially activated by intracellular calcium $[Ca_i^{2+}]$. In this section, we assume that the enzymatic activity of each enzyme can be represented as a function of $[Ca_i^{2+}]$ (Fig. 3), and that at lower $[Ca^{2+}]$, phosphatases are more activated than kinases, while at higher $[Ca^{2+}]$, kinases are more activated than phosphatases.

The phosphorylation cycle shown in Figure 2, which assumes two phosphorylation sites on GluR1, is composed of four reactions:

$$A \underset{P1}{\overset{K1}{\rightleftarrows}} A_{\mathrm{p1}},\ A^{\mathrm{p2}} \underset{P1}{\overset{K1}{\rightleftarrows}} A_{\mathrm{p1}}^{\mathrm{p2}},\ A \underset{P2}{\overset{K2}{\rightleftarrows}} A^{\mathrm{p2}},\ A_{\mathrm{p1}} \underset{P2}{\overset{K2}{\rightleftarrows}} A_{\mathrm{p1}}^{\mathrm{p2}}. \tag{1}$$

Where A, A_{p1}, A^{p2}, and $A_{\mathrm{p1}}^{\mathrm{p2}}$ denote, respectively, the AMPAR not phosphorylated, phosphorylated at p1 (=S831), at p2 (=S845), and double phosphorylated. This kinetic scheme (Fig. 2) can be described mathematically by applying the first order Mass Action approach, which leads to the following system:

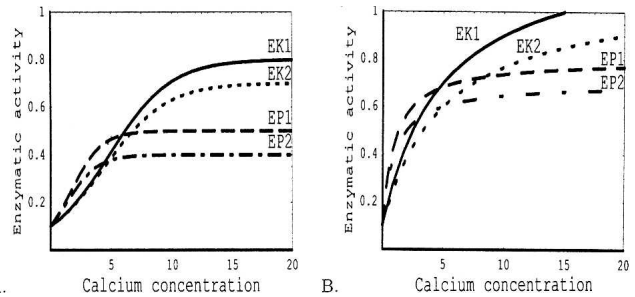

Figure 3. Kinase/phosphatase activation functions. (*A*) The calcium dependence of the activity of each of the four postsynaptic enzymes represented by a sigmoidal Hill function that takes into account the cooperative binding of calcium. (*B*) The calcium dependence of the activity of each of the four postsynaptic enzymes represented by a Michaelis-Menten function. Calcium concentration in arbitrary units.

$$\begin{pmatrix} \dot{A} \\ \dot{A}\mathrm{p1} \\ \dot{A}^{\mathrm{p2}} \\ \dot{A}^{\mathrm{p2}}_{\mathrm{p1}} \end{pmatrix} = \begin{pmatrix} -(K1+K2) & P1 & P2 & 0 \\ K1 & -(P1+K2) & 0 & P2 \\ K2 & 0 & -(P2+K1) & P1 \\ 0 & K2 & K1 & -(P1+P2) \end{pmatrix} \begin{pmatrix} A \\ A_{\mathrm{p1}} \\ A^{\mathrm{p2}} \\ A^{\mathrm{p2}}_{\mathrm{p1}} \end{pmatrix} \tag{2}$$

This system, by construction, keeps constant the total amount of protein:

$$\frac{dA}{dt} + \frac{dA^{\mathrm{p2}}}{dt} + \frac{dA_{\mathrm{p1}}}{dt} + \frac{dA^{\mathrm{p2}}_{\mathrm{p1}}}{dt} = 0 \Rightarrow A(t) + A^{\mathrm{p2}}(t) + A_{\mathrm{p1}}(t) + A^{\mathrm{p2}}_{\mathrm{p1}}(t) = A_T \tag{3}$$

A more compact form for the system (equation 2) is $\dot{\mathcal{A}} = \mathcal{S}\mathcal{A}$ where $\mathcal{A} = (A, A_{\mathrm{p1}}, A^{\mathrm{p2}}, A^{\mathrm{p2}}_{\mathrm{p1}})$ is the "state vector" of the AMPA receptors and $\mathcal{S}$ is the "coefficients" matrix. We observe that the system (equation 2) becomes a linear system if we consider that the time course of the calcium activation of the enzymes is much faster than the phospho/dephosphorylation time of GluR1, and the time-dependent solutions can be easily obtained by calculation of $\exp(\mathcal{S}t)$. As an example, we report the solution for $A^{\mathrm{p2}}_{\mathrm{p1}}(t)$, given a constant level of calcium:

$$A^{\mathrm{p2}}_{\mathrm{p1}}(t) = \frac{A_T \cdot K2 \cdot K1}{(K2+P2)\cdot(K1+P1)} + C_1 \cdot e^{\lambda 1 t} + C_2 \cdot e^{\lambda 2 t} + C_3 \cdot e^{\lambda 3 t}. \tag{4}$$

with $\lambda_1 = -(K1+P1)$, $\lambda_2 = -(K2+P2)$, $\lambda_3 = -(K1+K2+P1+P2)$, the eigenvalues of the $\mathcal{S}$ matrix, and C_1, C_2, C_3 are constants set by the initial conditions. Note that, in general, the kinetic constants ($K1$, $K2$, $P1$, $P2$) are calcium-dependent activity levels of the kinases and phosphatases, respectively, so that the equations time constants and steady-state solutions are calcium dependent as well.

We observe that $A^{\mathrm{p2}}_{\mathrm{p1}}(t)$ is composed of two parts, one not dependent on time (steady-state solution), and one that is time dependent (transient component). Characterization of the steady-state solution does not require explicit integration of the system (equation 2), and can be generalized to more complex situations. The kernel of the matrix $\mathcal{S}$ is nontrivial because $\mathcal{S}$ is, by construction, a singular matrix; a basis for this kernel is:

$$\vec{B}_{Ker(S)} = \left(\frac{M_1}{M_4} \quad \frac{M_2}{M_4} \quad \frac{M_3}{M_4} \quad 1\right) \tag{5}$$

where

$$M_1 = P1\cdot P2\cdot P2 + K1\cdot P2\cdot P1 + P1\cdot P2\cdot K1 + K2\cdot P2\cdot P1$$

$$M_2 = K1\cdot P2\cdot P2 + K1\cdot P2\cdot K1 + K1\cdot P1\cdot P1 + P2\cdot K2\cdot K1$$

$$M_3 = K2\cdot K2\cdot P1 + P1\cdot K2\cdot P1 + P1\cdot P2\cdot K2 + K1\cdot K2\cdot P1$$

$$M_4 = K1\cdot K2\cdot K1 + K2\cdot K2\cdot K1 + K1\cdot K2\cdot P2 + P1\cdot K2\cdot K1.$$

Now, by imposing the conservation of the total amount of protein (equation 3) we obtain the equilibrium solutions of (equation 2) as a fraction of A_T:

$$\begin{pmatrix} A_\infty \\ A_{\mathrm{p1}\infty} \\ A^{\mathrm{p2}}{}_\infty \\ A^{\mathrm{p2}}_{\mathrm{p1}\infty} \end{pmatrix} = \begin{pmatrix} \frac{M_1\cdot A_T}{M_1+M_2+M_3+M_4} \\ \frac{M_2\cdot A_T}{M_1+M_2+M_3+M_4} \\ \frac{M_3\cdot A_T}{M_1+M_2+M_3+M_4} \\ \frac{M_4\cdot A_T}{M_1+M_2+M_3+M_4} \end{pmatrix} = \begin{pmatrix} \frac{P1\cdot P2\cdot A_T}{(K1+K2)\cdot(P1+P2)} \\ \frac{K1\cdot P2\cdot A_T}{(K1+K2)\cdot(P1+P2)} \\ \frac{K2\cdot P1\cdot A_T}{(K1+K2)\cdot(P1+P2)} \\ \frac{K1\cdot K2\cdot A_T}{(K1+K2)\cdot(P1+P2)} \end{pmatrix}. \tag{6}$$

This approach can be generalized to the case of a nonspecific phosphatase $P2 \equiv P1$ and it gives relations similar to equation 6.

We will concentrate on the behavior of the $A^{\mathrm{p2}}_{\mathrm{p1}}(t)$ solution, and how the solution depends on assumptions regarding the calcium dependence of the enzymes involved in the pathway. We compare two quantitatively different sets of assumptions as follows: (1) The activity of each enzyme shows a sigmoidal dependence on Ca^{2+}, but with different sensitivity to the concentration; this type of dependence will be described by a Hill-type function

$$f(Ca) = \frac{Ca^h}{k^h + Ca^h}$$

$h > 1$ (Fig. 3A); (2) the activity of each enzyme shows a Michaelis-Menten dependence on $[Ca^{2+}_i]$, but with different affinity constants:

$$k_m(Ca)\colon \upsilon = \frac{k_{irr} E_T Ca}{k_m + Ca}$$

(Fig. 3B), where v is the velocity of product formation.

The behavior of the solutions (equation 6) in the cases of two phosphatases and two kinases is shown in Figure 4, where we use the Michaelis Menten and the Hill function, respectively. Qualitatively, the two cases have a similar form. At low calcium levels, they exhibit LTD, whereas at higher levels, they exhibit

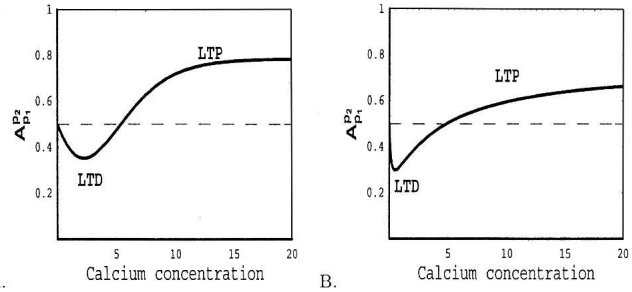

Figure 4. Levels of the double phosphorylated (A^{p2}_{p1}) state of AMPAR as a function of postsynaptic calcium concentration. Each graph represents an equilibrium solution obtained by the mass-action approach (equation 2). Low levels of A^{p2}_{p1} imply LTD and high levels imply LTP. (*A*) Levels of A^{p2}_{p1} state of AMPAR when the calcium dependence of each of the phosphorylation/dephosphorylation reactions is represented by a sigmoidal Hill function. (*B*) Levels of (A^{p2}_{p1}) state of AMPAR when the calcium dependence of each of the phosphorylation/dephosphorylation reactions is represented by a hyperbolic Michaelis-Menten function. Calcium concentration in arbitrary units.

LTP. However, quantitative differences are significant. For example, the LTD region resulting from the Michaelis-Menten curves occurs at a significantly lower value of $[Ca_i^{2+}]$, the magnitudes of the $A_{\mathrm{p1}}^{\mathrm{p2}}$ state increase more gradually and saturate at higher calcium levels. Synaptic strength is related to the phosphorylation state of GluR1, since phosphorylation at both sites increases the average AMPAR conductance level by approximately twofold. If mechanisms for phosphorylation at each site are independent, conductance approximately follows the following equation conductance $\propto (A + 2^{*} (A_{p1} + A^{p2}) + 4A_{p1}^{p2}$ (Castellani et al. 2001). We used this equation above to estimate the conductance in arbitrary units.

Analysis of the AMPAR cycle by Michaelis–Menten kinetics

For a more accurate description of AMPAR phosphorylation/dephosphorylation cycle (Fig. 2), we use the Michaelis-Menten approach. Here, the effect of each enzyme is described as a combination of reversible and nonreversible reactions, making the standard pseudo-steady state assumptions (Segel 1975). Hence, with two phosphorylation sites and four different enzymes, this cycle takes the following form:

$$
\begin{aligned}
K1 + A &\underset{\kappa_b^1}{\overset{\kappa_f^1}{\rightleftarrows}} K1A \xrightarrow{\kappa_{irr}^1} K1 + A_{\mathrm{p1}} \quad ; \\
P1 + A_{\mathrm{p1}} &\underset{\kappa_b^2}{\overset{\kappa_f^2}{\rightleftarrows}} P1A_{\mathrm{p1}} \xrightarrow{\kappa_{irr}^2} P1 + A \\
K2 + A_{\mathrm{p1}} &\underset{\kappa_b^3}{\overset{\kappa_f^3}{\rightleftarrows}} K2A_{\mathrm{p1}} \xrightarrow{\kappa_{irr}^3} K2 + A_{\mathrm{p1}}^{\mathrm{p2}} \quad ; \\
P2 + A_{\mathrm{p1}}^{\mathrm{p2}} &\underset{\kappa_b^4}{\overset{\kappa_f^4}{\rightleftarrows}} P2A_{\mathrm{p1}}^{\mathrm{p2}} \xrightarrow{\kappa_{irr}^4} P2 + A_{\mathrm{p1}} \\
K2 + A &\underset{\kappa_b^5}{\overset{\kappa_f^5}{\rightleftarrows}} K2A \xrightarrow{\kappa_{irr}^5} K2 + A^{\mathrm{p2}} \quad ; \\
P2 + A^{\mathrm{p2}} &\underset{\kappa_b^6}{\overset{\kappa_f^6}{\rightleftarrows}} P2A^{\mathrm{p2}} \xrightarrow{\kappa_{irr}^6} P2 + A \\
K1 + A^{\mathrm{p2}} &\underset{\kappa_b^7}{\overset{\kappa_f^7}{\rightleftarrows}} K1A^{\mathrm{p2}} \xrightarrow{\kappa_{irr}^7} K1 + A_{\mathrm{p1}}^{\mathrm{p2}} \quad ; \\
P1 + A_{\mathrm{p1}}^{\mathrm{p2}} &\underset{\kappa_b^8}{\overset{\kappa_f^8}{\rightleftarrows}} P1A_{\mathrm{p1}}^{\mathrm{p2}} \xrightarrow{\kappa_{irr}^8} P1 + A^{\mathrm{p2}}.
\end{aligned}
\tag{7}
$$

The constants k_f^{i}, k_b^{i}, k_{irr}^{i} $i = 1,\ldots 8$ are the rate constants for the forward, backward, and irreversible steps, respectively. According to the Michaelis-Menten analysis, we also define the Michaelis-Menten constants

$$
k_m^{\mathrm{i}} = \frac{k_b^{\mathrm{i}} + k_{irr}^{\mathrm{i}}}{k_f^{\mathrm{i}}}, \; i = 1, \ldots 8.
$$

The pseudo-steady state hypothesis sets to zero the derivatives of all the enzyme-substrate complexes as follows: $\dot{K1A} = \dot{P1A}_{\mathrm{p1}} = \dot{K2A}_{\mathrm{p1}} = \dot{P2A}_{\mathrm{p1}}^{\mathrm{p2}} = \dot{K2A} = \dot{P2A}^{\mathrm{p2}} = \dot{K1A}^{\mathrm{p2}} = \dot{P1A}_{\mathrm{p1}}^{\mathrm{p2}} = 0$. The conservation law for each enzyme sets the total amount of each enzyme as a constant as follows: $K1 + K1A + K1A^{\mathrm{p2}} = K1_T$; $P1 + P1A_{\mathrm{p1}} + P1A_{\mathrm{p1}}^{\mathrm{p2}} = P1_T$; $K2 + K2A + K2A_{\mathrm{p1}} = K2_T$; $P2 + P2A^{\mathrm{p2}} + P2A_{\mathrm{p1}}^{\mathrm{p2}} = P2_T$.

This approach allows us to write a compact representation for the concentrations of the different fractions of AMPAR:

$$
\dot{\mathcal{A}} = \mathcal{R}\mathcal{A}; \tag{8}
$$

where $\mathcal{A} = (A, A_{\mathrm{p1}}, A^{\mathrm{p2}}, A_{\mathrm{p1}}^{\mathrm{p2}})$, and $\mathcal{R}$ is a "coefficients matrix":

$$
\mathcal{R} = \begin{pmatrix}
-(c_1F_{K1} + c_2F_{K2}) & c_3F_{P1} & c_4F_{P2} & 0 \\
c_1F_{K1} & -(c_5F_{K2} + c_3F_{P1}) & 0 & c_6F_{P2} \\
c_2F_{K2} & 0 & -(c_7F_{K1} + c_4F_{P2}) & c_8F_{P1} \\
0 & c_5F_{K2} & c_7F_{K1} & -(c_8F_{P1} + c_6F_{P2})
\end{pmatrix} \tag{9}
$$

with:

$$
\begin{aligned}
&c_1 = k_{irr}^1 \cdot k_m^7,\; c_2 = k_{irr}^5 \cdot k_m^3,\; c_3 = k_{irr}^2 \cdot k_m^8,\; c_4 = k_{irr}^6 \cdot k_m^4, \\
&c_5 = k_{irr}^3 \cdot k_m^5,\; c_6 = k_{irr}^4 \cdot k_m^6,\; c_7 = k_{irr}^7 \cdot k_m^1,\; c_8 = k_{irr}^8 \cdot k_m^2
\end{aligned} \tag{10}
$$

and the four "fluxes" have the form

$$
\begin{aligned}
&\mathcal{F}_{K1} = \frac{K1_T}{k_{m1}k_{m7} + k_{m1}A^{\mathrm{p2}} + k_{m7}A} \;;\; \mathcal{F}_{P1} = \frac{P1_T}{k_{m2}k_{m8} + k_{m2}A_{\mathrm{p1}}^{\mathrm{p2}} + k_{m8}A_{\mathrm{p1}}} \\
&\mathcal{F}_{K2} = \frac{K2_T}{k_{m3}k_{m5} + k_{m3}A + k_{m5}A_{\mathrm{p1}}} \;;\; \mathcal{F}_{P2} = \frac{P2_T}{k_{m4}k_{m6} + k_{m4}A^{\mathrm{p2}} + k_{m6}A_{\mathrm{p1}}^{\mathrm{p2}}}.
\end{aligned} \tag{11}
$$

Note that equation 8 has a form similar to the first order mass action equation (equation 2); however, there is a significant difference in that the "fluxes" are not constant, but are functions of the dynamic variables. Thus, this equation is nonlinear and a full solution of the dynamics has not been analytically obtained. In order to characterize the fixed points, we observe that the matrix $\mathcal{R}$ has a nontrivial Kernel, hence, a vector basis of $Ker(\mathcal{R})$ is:

$$
\vec{B}_{Ker(\mathcal{R})} = \left(\frac{\mathcal{D}_1}{\mathcal{D}_4}, \frac{\mathcal{D}_2}{\mathcal{D}_4}, \frac{\mathcal{D}_3}{\mathcal{D}_4}, 1\right) \tag{12}
$$

where:

$$
\begin{aligned}
\mathcal{D}_1 &= c_3c_6c_7\mathcal{F}_{P1}\mathcal{F}_{P2}\mathcal{F}_{K1} + c_3c_4c_6\mathcal{F}_{P1}\mathcal{F}_{P2}\mathcal{F}_{P2} + c_4c_5c_8\mathcal{F}_{K2}\mathcal{F}_{P2}\mathcal{F}_{P1} \\
&\quad + c_3c_4c_8\mathcal{F}_{P1}\mathcal{F}_{P2}\mathcal{F}_{P1} \\
\mathcal{D}_2 &= c_1c_6c_7\mathcal{F}_{K1}\mathcal{F}_{K1}\mathcal{F}_{P2} + c_2c_6c_7\mathcal{F}_{K2}\mathcal{F}_{K1}\mathcal{F}_{P2} + c_1c_4c_6\mathcal{F}_{K1}\mathcal{F}_{P2}\,\mathcal{F}_{P2} \\
&\quad + c_1c_4c_8\mathcal{F}_{K1}\mathcal{F}_{P2}\mathcal{F}_{P1} \\
\mathcal{D}_3 &= c_2c_5c_6\mathcal{F}_{P2}\mathcal{F}_{K2}\mathcal{F}_{K2} + c_2c_3c_8\mathcal{F}_{P1}\mathcal{F}_{K2}\mathcal{F}_{P1} + c_2c_5c_6\mathcal{F}_{P2}\mathcal{F}_{K2}\mathcal{F}_{K2} \\
&\quad + c_1c_5c_8\mathcal{F}_{K1}\mathcal{F}_{K2}\mathcal{F}_{P1} \\
\mathcal{D}_4 &= c_1c_5c_7\mathcal{F}_{K1}\mathcal{F}_{K2}\mathcal{F}_{K1} + c_2c_5c_7\mathcal{F}_{K2}\mathcal{F}_{K2}\mathcal{F}_{K1} + c_2c_3c_7\mathcal{F}_{P1}\mathcal{F}_{K2}\mathcal{F}_{K1} \\
&\quad + c_1c_4c_5\mathcal{F}_{K1}\mathcal{F}_{K2}\mathcal{F}_{P2}
\end{aligned}
$$

This permits us to write the equilibrium solutions, in a form that is similar to equation 6.

$$
\begin{aligned}
\begin{pmatrix} A(\infty) \\ A_{\mathrm{p1}}(\infty) \\ A^{\mathrm{p2}}(\infty) \\ A_{\mathrm{p2}}^{\mathrm{p1}}(\infty) \end{pmatrix} &= \begin{pmatrix}
\dfrac{\mathcal{D}_1 \cdot \mathcal{A}_T}{\mathcal{D}_1 + \mathcal{D}_2 + \mathcal{D}_3 + \mathcal{D}_4} \\
\dfrac{\mathcal{D}_2 \cdot \mathcal{A}_T}{\mathcal{D}_1 + \mathcal{D}_2 + \mathcal{D}_3 + \mathcal{D}_4} \\
\dfrac{\mathcal{D}_3 \cdot A_T}{\mathcal{D}_3 + \mathcal{D}_2 + \mathcal{D}_3 + \mathcal{D}_4} \\
\dfrac{\mathcal{D}_4 \cdot \mathcal{A}_T}{\mathcal{D}_1 + \mathcal{D}_2 + \mathcal{D}_3 + \mathcal{D}_4}
\end{pmatrix} \\
&= \begin{pmatrix}
\dfrac{\mathcal{F}_{P1} \cdot \mathcal{F}_{P2} \cdot A_T}{(\mathcal{F}_{P1} + \mathcal{F}_{K1}) \cdot (\mathcal{F}_{P2} + \mathcal{F}_{K2})} \\
\dfrac{\mathcal{F}_{K1} \cdot \mathcal{F}_{K2} \cdot A_T}{(\mathcal{F}_{P1} + \mathcal{F}_{K1}) \cdot (\mathcal{F}_{P2} + \mathcal{F}_{K2})} \\
\dfrac{\mathcal{F}_{P1} \cdot \mathcal{F}_{K2} \cdot A_T}{(\mathcal{F}_{P1} + \mathcal{F}_{K1}) \cdot (\mathcal{F}_{P2} + \mathcal{F}_{K2})} \\
\dfrac{\mathcal{F}_{K1} \cdot \mathcal{F}_{K2} \cdot A_T}{(\mathcal{F}_{P1} + \mathcal{F}_{K1}) \cdot (\mathcal{F}_{P2} + \mathcal{F}_{K2})}
\end{pmatrix}.
\end{aligned} \tag{13}
$$

This relation allows us to compute the "Fluxes" in various cases, even when two specific kinases ($K1$, $K2$) and only one phosphatase $P1$ are present. Here, we can calculate the constants $c_1,c_2,\ldots,c_8$ and define three "Fluxes" $\mathcal{F}_{K1}$, $\mathcal{F}_{K2}$, $\mathcal{F}_{P1}$.

From these solutions, we can characterize the phosphorylation state of the various AMPAR fractions as a function of enzymatic activity. When the phosphatases (P1, P2) are activated above basal levels, the equilibrium will shift toward a state in which the fraction of A is greater than the others. When the kinases (K1, K2) are activated above basal levels, the A^{p2}_{p1} fraction will be predominant. An asymmetric situation occurs when there is activation of one kinase and one phosphatase (K1 P2) or (K2 P1), in which an increase of A^{p2} or A_{p1} fractions takes place. The synchronous activation of all of the enzymes to the same level of activity will generate a state in which all of the AMPAR fractions are at the same concentration.

Calcium dependence of enzymatic activity

The Michaelis-Menten approach can be extended to account for the calcium dependence of the enzymes. We consider again four enzymes, K1, P1, K2, and P2, that are activated by calcium with the reactions

$$ECa_s + Ca \underset{K_{D_s}}{\overset{K_{A_s}}{\rightleftarrows}} ECa_{s+1} \tag{14}$$

where the subscript s denotes the number of Ca molecules bound to E, here $s = 0,\ldots,3$, and where k_{A_s}, k_{D_s}, and k_{E_s} are the association, the dissociation, and the equilibrium constant for each reaction. With these assumptions (see Appendix), we can define a saturation curve σ_i that relates $[Ca^{2+}]$ to the activity of each enzyme (see Appendix). These functions are sigmoidal (Hill-like functions) because the process is cooperative. Previous derivations assumed that the enzymes become fully activated by binding four molecules of calcium, and we will adopt the same assumptions. The approach of equations 6–13 can be applied here to obtain the calcium dependent fluxes:

$$\mathcal{F}^{Ca}_{K1} = \frac{K1_T \cdot \sigma_{K1}(Ca)}{k^1_m k^7_m + k^1_m \cdot \sigma_{K1}(Ca)A^{P2} + k^7_m \cdot \sigma_{K1}(Ca)A};$$

$$\mathcal{F}^{Ca}_{P1} = \frac{P1_T \sigma_{P1}(Ca)}{k^2_m k^8_m + k^2_m \sigma_{P1}(Ca)A^{p2}_{p1} + k^8_m \sigma_{P1}(Ca)A_{p1}}$$

$$\mathcal{F}^{Ca}_{K2} = \frac{K2_T \sigma_{K2}(Ca)}{k^3_m k^5_m + k^3_m \sigma_{K2}(Ca)A + k^5_m \sigma_{K2}(Ca)A_{p1}};$$

$$\mathcal{F}^{Ca}_{P2} = \frac{P2_T \sigma_{P2}(Ca)}{k^4_m k^6_m + k^4_m \sigma_{P2}(Ca)A^{p2} + k^6_m \sigma_{P2}(Ca)A^{p2}_{p1}},$$

where the σ_i, $i \in (K1, K2, P1, P2)$ are the saturation functions for the calcium binding of each enzyme:

$$\sigma_i = \frac{(Ca)^4}{k_{E_{0j}} k_{E_{1j}} k_{E_{2j}} k_{E_{3j}} + k_{E_{1j}} k_{E_{2j}} k_{E_{3j}} \cdot Ca + k_{E_{2j}} k_{E_{3j}} \cdot (Ca)^2 + k_{E_{3j}} \cdot (Ca)^3 + (Ca)^4};$$

$$i = j \in \{K1, K2, P1, P2\}.$$

With this formalism, we can rewrite the system as

$$\dot{\mathcal{A}} = \mathcal{P}\mathcal{A} \tag{15}$$

where the matrix $\mathcal{P}$ is formally similar to the matrix $\mathcal{R}$ of equation 9, but the fluxes F_j are substituted by the calcium-dependent fluxes F^{Ca}_j. The structure of these equations is similar to that of equations 2 and 8 because, again, the total amount of AMPAR protein is conserved ($A + A^{p2} + A_{p1} + A^{p2}_{p1} = A_T$). The matrix formed by the "calcium-dependent fluxes" has a nontrivial kernel, thus, again, we can apply the fixed point analysis. In this case, it is not possible to find a closed form solution, and we will therefore examine the behavior of the solutions by numerical integration of equation 15. Our interest is to characterize the fixed point as a function of $[Ca^{2+}_i]$, and therefore, we numerically integrate the system with different levels until it reaches the stable fixed point. The results are illustrated in Figure 5. In comparison to Figure 4, this approach results in a solution with larger LTP and LTD and a sharper transition between LTP and LTD. Therefore, it seems that the Michaelis-Menten approach results in more robust synaptic plasticity. The results depicted here in Figures 4, 5, and 7, below, are the steady-state solutions for a prolonged elevation of calcium level. These results cannot be easily compared with experimental results in which LTP and LTD are induced by protocols that produce transient changes in calcium concentration. In a previous work (Shouval et al. 2002b), we obtained a rule that can be applied to induction of plasticity with calcium transients. The rule extracted by Shouval et al. (2002b) gives the derivative of the synaptic weight as a function of instantaneous calcium. This seems qualitatively similar to results predicted by BCM theory (Bienenstock et al. 1982), but depends on calcium rather then on pre- and postsynaptic activity. We have previously translated the biophysical model to be a function of pre- and postsynaptic activity (Castellani et al. 2001; Shouval et al. 2002b); there, however, we find that, unlike BCM, the plasticity equations are no longer linear in presynaptic activity. These differences from the BCM theory, which result from this more detailed biophysical modeling, are to be expected, and the consequences of these detailed differences are currently under investigation (Yeung et al. 2004).

A detailed enzymatic model

In the previous section, we have shown that our biophysical model can qualitatively account for the calcium dependence of the phosphorylation state of AMPAR under a set of mild assumptions. In this section, we ask whether this set of assumptions is applicable to real cortical neurons. To do this, we introduce a more detailed model of the $[Ca^{2+}_i]$ dependence of each enzyme (Fig. 6). In addition, we ask whether the more detailed enzymatic model results in more specific physiological and biophysical consequences. This scheme differs from one described in the previous section, in that we have named specific enzymes as responsible for phosphorylation and dephosphorylation of GluR1.

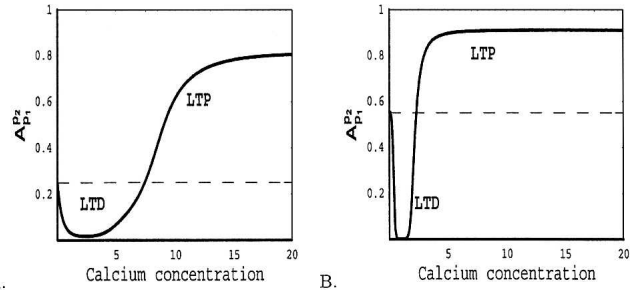

Figure 5. Levels of the (A^{p2}_{p1}) using the Michaelis-Menten approach. Each graph depicts equilibrium solutions obtained by numerical integration (equation 15) with two Kinases and two Phosphatases. (*A*) Levels of the (A^{p2}_{p1}) state of AMPAR when the calcium dependence of each of the phosphorylation/dephosphorylation reactions is represented by a sigmoidal Hill function (as in Fig. 3A). (*B*) Levels of (A^{p2}_{p1}) state of AMPAR when the calcium dependence of each of the phosphorylation/dephosphorylation reactions is represented by a hyperbolic Michaelis-Menten function (as in Fig. 3B). Calcium concentration in arbitrary units.

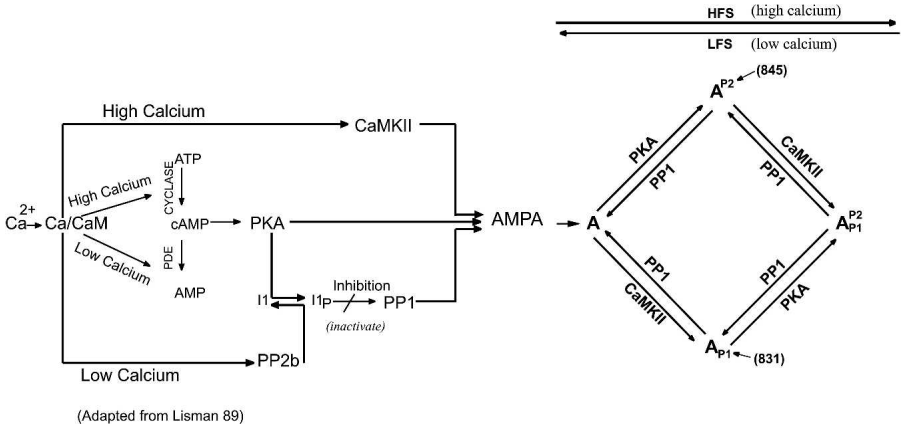

Figure 6. Calcium-dependent activity of the kinase/phosphatase network. (*Left*) Introduction of specific activity-dependent protein kinases and protein phosphatases into the schematic representation of bidirectional phosphorylation/dephosphorylation of the GluR1 subunit of the AMPAR. A schematic description of the calcium-dependent signal transduction cascades that regulate AMPA receptor phosphorylation. An increase in postsynaptic calcium concentration results in an increase in postsynaptic calcium–calmodulin (Ca–CaM) concentration. Low levels of Ca–CaM stimulate PP2b activity directly, while higher levels of Ca–CaM stimulate CaMKII activity. PKA and PP1 are indirectly regulated by calcium. PKA is activated by camp, which can be generated by calcium-dependent adenylyl cyclase (AC) and degraded by phosphodiesterase (PDE). PP1 activity level is inhibited by the protein inhibitor 1/DARPP32 (I_1). The inhibition is released by dephosphorylation of inhibitor 1/DARPP32 via the activity of PP2b. (Modified from Lisman 1989). (*Right*) There are two phosphorylation sites on the GluR1 subunit of the AMPAR, serine 845 (S845) and serine 831 (S831). S845 is phosphorylated by protein kinase A (PKA) and dephosphorylated by protein phosphatase 1 (PP1); S831 is phosphorylated by calcium–calmodulin-dependent protein kinase II (CaMKII) and dephosphorylated by protein phosphatase 1 (PP1). High-frequency stimulation of the synapses (HFS) results in a large increase in postsynaptic calcium, and a resultant activation of the calcium–calmodulin-dependent protein kinases. Low-frequency stimulation of the synapse (LFS) results in a modest increase in postsynaptic calcium and a resultant activation of the calcium–calmodulin-dependent protein phosphatases. Modified from Kameyama et. al (1998).

Phosphorylation of S845 is mediated by PKA, and phosphorylation of S831 can be mediated by CaMKII and PKC. Since the pathway leading from calcium concentration to CaMKII activation is well resolved, we have found that it is sufficient to assume phosphorylation at S831 by CaMKII. Pharmacologically blocking either PP2b or PP1 can inhibit LTD induction (Mulkey et al. 1994). PP1 is thought to dephosphorylate S831 and S845, and PP1 activation is indirectly dependent on $[Ca_i^{2+}]$. The activation of PP2B by calcium results in dephosphorylation of inhibitor 1 (I_1), and disinhibition of PP1. Thus, three enzymes are assumed to interact directly with the AMPAR, i.e., CaMKII, PKA, and PP1 (Fig. 6, right). In this section, we model the signal transduction cascade leading from an increase in $[Ca_i^{2+}]$ to the activation levels of the three key enzymes. A schematic diagram of the signal transduction cascades affecting these enzymes is displayed in Figure 6. Of these three enzymes, only CaMKII depends directly on the concentration of the calcium–calmodulin complex (Ca–CaM). PKA activity level is camp dependent, which is degraded by phosphodiesterase (PDE) and stimulated by adenylate cyclase (AC), both of which are modulated by calcium. A simple mass-action approach to this reaction results in the following steady state formula: $cAMP = AC/PDE$. PP1 activity depends indirectly on calcium because it is inhibited by the phosphorylated form of inhibitor 1 (I_1). Inhibitor 1 is phosphorylated by PKA and dephosphorylated by PP2b. Therefore, $[Ca_i^{2+}]$-dependent activation of PP2B results in dephosphorylation of $I1$ and activation of PP1. A simple mass-action approach, following Lisman (1989), produces the following result: $I1 = 0.1 * PKA/(PKA = PP2b)$, where 0.1 is the maximal activation level of $I1$. The fraction of bound PP1 is assumed to be $f = I_1/(I1 + 0.001)$ (Lisman 1989) and, therefore, the active level of PP1 is $PP1 = 1 - f$.

After making these assumptions, the remaining kinetic coefficients (such as $k_{1/2}$) for the $[Ca_i^{2+}]$ activation of each enzyme were extracted from the literature. Some kinetic coefficients were determined by a direct measurement or control of calcium (at high levels of CaM), while other experiments measured Ca–CaM (Calcium Calmodulin complex), by manipulating CaM levels (at a given high calcium concentration).

In order to translate the results obtained using the Ca–CaM approach, we use the result of Persechini and Cronk (1999), who measured the dependence of Ca–CaM on intracellular calcium concentration. They have shown that the level of Ca–Cam can be expressed as a function of Ca and the total amount of Calmodulin in the cell

$$Ca - CaM = K \frac{Ca^{2.6}}{k_{1/2}^{2.6} + Ca^{2.6}}$$

where K is a parameter related to total CaM in the spine, which is regarded as an isolated compartment. It is reasonable to assume biologically realistic parameters, in which the maximum concentration of *Ca–CaM* is ~45 nM, the constant $k_{1/2}$ is 1 μM, the Hill coefficient is ~2.6, and K can range from 10 to 40 nM. In Table 1, we list our assumptions about each kinetic coefficient. The experimental data often give good estimates for $k_{1/2}$ and sometimes for the Hill coefficient h; moreover, the results are typically not sensitive to the value of h. The values of the maximal activity level of each enzyme listed in Table 1 (V_{max}), and the basal activity level (V_{base}) cannot be extracted from the experimental data, as these depend critically on total enzyme concentration in vivo. We have chosen the parameters similar to that observed in vivo and to obtain reasonable results. In Figure 7, we display results using kinetic coefficients for direct calcium dependence (left) and Ca–CaM dependence (right). In Figure 7, A and D, the activity levels of the three directly interacting enzymes *CaM KII*, *PKA*, and *PP*1 are displayed relative to intracellular concentration of calcium (left) or calcium–calmodulin (right). In Figure 7, B and E, the fraction of AMPARs in each of the different phosphorylation states is displayed, and in Figure 7, C and F, an estimate of the total conductance is shown. The conductance is estimated, as above by: $conductance = A + 2(A_{p1} + A^{p2}) + 4A_{p1}^{p2}$. Although the detailed assumptions about enzymatic activity are quantitatively quite different, both approaches produce an LTP/LTD curve with depression at moderate calcium levels and potentiation at high calcium levels. A critical parameter in determining the conductance at basal calcium levels is V_{base}, the basal activity level of each enzyme. For each enzyme, the value of V_{base} is low; however, at such low basal levels, small differences in calcium concentration can have a large effect on the results. We have chosen values of V_{base} to attain intermediate values of AMPAR conductance at baseline. In addition, we have chosen the values of V_{base} so that at baseline, S845 would be more highly phosphorylated than the S831, consistent with experimental reports (Lee et al. 2000b). In general, the phosphorylation curves (Fig. 7B,E) are more constraining than the conductance plots (Fig. 7C,F), since

Table 1. Kinetic coefficients for relevant enzymes

Enzyme	Ca–CaM dependence	Direct Ca dependence
CaMKII	$K_{1/2}$ = 45 nM (Meyer et al. 1992) V_{max} = 10 V_{base} = .005 h = 4	→ $K_{1/2}$ = 1.5 μM V_{max} = 1 V_{base} = .005 h = 4
PP2b	$k_{1/2}$ = 0.1 − 1 nM (Stemmer and Klee 1994; Wang and Kelly 1997) V_{max} = 1 V_{base} = 0.01 h = 3	→ $k_{1/2}$ = 0.1–0.25 μM V_{max} = 1 V_{base} = 0.01 h = 3
PDE	$k_{1/2}$ = 0.1 nM (Klee and Cohen 1988) V_{max} = 1 V_{base} = .01 h = 2	$k_{1/2}$ = 2.5 μM (Gu and Cooper 2000) V_{max} = 1 μM V_{base} = .1
AC	$k_{1/2}$ = 15 nM (Klee and Cohen 1988) V_{max} = 1 V_{base} = .01 h = 3	$k_{1/2}$ = .38 μM k_i = 132 μM* (Gu and Cooper 2000) V_{max} = 1 V_{base} = .01 h = 4
PKA	$k_{1/2}$ = 1 μM[a] (cAMP) (Huang and Taylor 1998) V_{max} = 5 V_{base} = .01 h = 2	$k_{1/2}$ = 1 μM[a] (*cAMP*) V_{max} = 1 V_{base} = .015 h = 2

Two approaches were used to extract kinetic coefficients from the literature to produce the calcium-dependence curves of each enzyme. Additional theoretical inferences for extracting the PP1 and cAMP dependence are described in the text. These enzymatic reactions typically have the form $V = V_{base} + V_{max}\, x^h/x^h + k_{1/2}^h$, where x is the activating factor, either Ca, or Ca–CaM. Notation: (→) The data was translated into the Ca column from the Ca–CaM column using the relation $CaCaM = CaM\ Ca^{2.6}/1 + Ca^{2.6}$ (Persechini and Cronk 1999); (*k_i), inactivation constant.
[a]PKA as a function of cAMP. All the velocities V_{max}, V_{base} and V are expressed in mol/min.

multiple configurations of the phosphorylation curves can produce the same conductance curves. A significant factor in both of the detailed models is that the PP1 activity curve is not a monotonic sigmoid, but is approximatively bell shaped. This differs from the assumptions we made for the abstract qualitative models. LTD occurs at low calcium levels, due to the peak in PP1 activity. Eliminating this peak in PP1 activity would abolish LTD. The shape of the PP1 curve depends on both PP2b and PKA activity. Thus, inhibiting PP1 directly or indirectly through PP2b inactivation would reduce the level of LTD, consistent with experimental observations (Mulkey et al. 1993, 1994). Our models are consistent with Lee et al. (2000b), who found that LTD, from baseline, produces dephosphorylation of S845 (PKA-site), and that LTP produces phosphorylation of S831 (CaMKII-site).

Both of our models exhibit phosphorylation of AMPA receptors at the S845 site at basal calcium levels, due to the assumption that PKA activity at basal calcium levels is greater than activity of PP1, PP2b, or CamKII. Examining this key assumption experimentally is a test for the validity of our detailed model.

Discussion

Changes in synaptic efficacy underlie many fundamental properties of nervous system function, such as developmental refinement of receptive fields, learning, and memory. As such, the molecular mechanisms underlying the regulation of synaptic strength have been an area of intense investigation. Here, we use experimentally derived properties of intracellular signaling cascades and postsynaptic glutamate receptor phosphorylation to model bidirectional regulation of synaptic strength. First, we demonstrate that knowledge of the activation coefficients of $[Ca^{2+}]$ requisite-dependent protein kinases and protein phosphatases is sufficient to predict activity-dependent phosphorylation/dephosphorylation of GluR1 and corresponding changes in the conductance of the AMPAR. We show that regulation of AMPAR phosphorylation can indeed qualitatively account for LTP/LTD curves observed experimentally, lending further support to the claim that phosphorylation of AMPAR is a primary substrate of bidirectional synaptic plasticity. This extends the experimental work that demonstrates a correlation between synaptic plasticity and AMPAR phosphorylation. This work supports and extends our previous model of bidirectional synaptic plasticity (Castellani et al. 2001), which was based on a simple, first order, mass-action approach by using a more precise and complex Michaelis-Menten approach. Both models result in qualitatively similar LTP/LTD curves. However, it is important to stress the differences between the types of predictions the two approaches can make. The simple first order mass-action approach can only make qualitative predictions, whereas the Michaelis-Menten approach can result in precise predictions, the accuracy of which is dependent on the precision of the kinetic coefficients.

In addition to improving the mathematical methodology, we have implemented a detailed model of the signal-transduction cascade leading from calcium influx in the postsynaptic neuron to AMPAR phosphorylation/dephosphorylation. This has produced LTP/LTD curves that are consistent with experimental results and consistent with our previous model. The quantitative aspects of our results stem from detailed assumptions about the calcium dependence of enzymatic activity, assumptions that, at this point, are not fully substantiated. The significance of these assumptions are revealed in Figure 7, in which the phosphorylation of GluR1 and the conductance of the AMPAR differ greatly, depending on whether direct $[Ca^{2+}]$ dependence or Ca^{2+}–CaM dependence is used to derive the enzymatic activity. Despite the different assumptions made in each model, we report that in all cases, LTD is induced by a moderate calcium increase and LTP is induced by high calcium concentrations.

Recent experimental results show that LTD is correlated with the phosphorylation of S845, whereas depotentiation (the reversal of LTP with low frequency stimulation) is correlated with dephosphorylation of S831 (Lee et al. 2000b). This could imply that S845 can only be dephosphorylated if S831 is not phosphorylated, thus, phosphorylation at these sites is not independent. Our model, which assumes two independent phosphorylation sites, points to an alternative explanation. If, as we assume, PKA activity levels are high at basal calcium levels, but CaMKII levels are not, then at baseline, S845 would tend to be phosphorylated. Hence, LTD from baseline would dephosphorylate S845. In contrast, after LTP, S831 would be phosphorylated, thus, the same paradigm that induces LTD from baseline, would in this case induce dephosphorylation at S831.

Our approach is motivated by Lisman's model (1989) of bidirectional synaptic plasticity. However, we consider phosphorylation/dephosphorylation regulation at AMPAR conductance, rather than activity-dependent regulation of CaMKII activity, as the primary mediator of LTP/LTD. While regulation of CaMKII activity, via CaMKII autophosphorylation, may be involved in

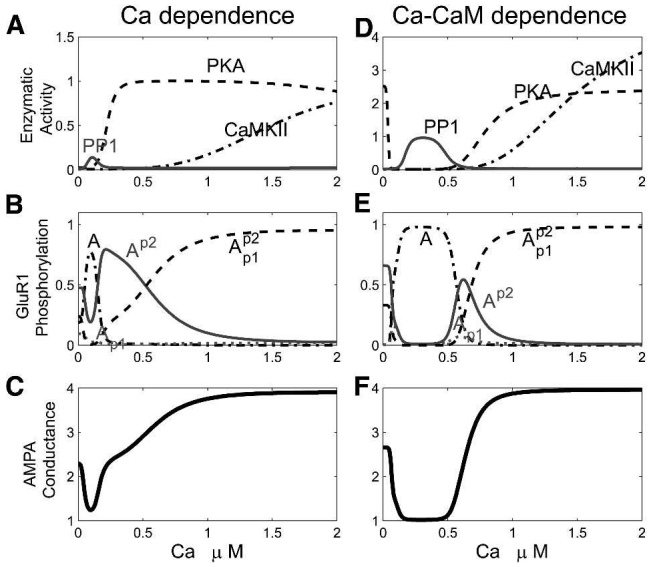

Figure 7. Levels of enzyme activity, GluR1 phosphorylation and AMPAR conductance as a function of postsynaptic calcium concentration. (*A*,*B*,*C*) Calculated from biochemical data with fixed calmodulin concentrations and varied calcium concentrations. (*D*,*E*,*F*) Calculated from data with fixed levels of calcium and varied levels of calmodulin. (*A*,*D*) Enzymatic activity (mol/min) as a function of postsynaptic calcium concentration. In both cases, the activation of PP1 is achieved at low concentrations, and the activation of PKA and CaMKII is achieved at higher concentrations. In *A*, the range of postsynaptic calcium concentrations that activate PP1 is very narrow, whereas in *B* there is a wider range of postsynaptic calcium concentrations that results in activation of PP1. Intermediate concentrations result in activation of PKA and high concentrations result in activation of CaMKII. (*B*,*E*) The resulting phosphorylation state (expressed as percentage of the total) of the GluR1 subunit of the AMPAR as a function of postsynaptic calcium concentration. The shape of the four curves in each graph is qualitatively similar. The most significant difference is that the range over which *A* is dominant is broader in the Ca–Calmodulin-based case. (*C*,*F*) Translating changes in AMPAR phosphorylation to AMPAR conductance (in arbitrary unit) gives qualitatively similar results when considering the dependence on $[Ca_i^{2+}]$. AMPAR conductance is lower than baseline levels at low concentrations of intracellular Ca or Ca–CaM, and reaches a maximal plateau level at ~1 uM. The interesting differences are in the shapes of the curves, with a gradual increase in conductance when considering only the Ca dependence and a less gradual increase when considering Ca–CaM.

the long-term maintenance of synaptic potentiation (but, see, Otmakhov et al. 1997), we did not include this in our models, since, here, we focus on early postsynaptic signaling events involved in the induction of LTP/LTD.

In our approach, we have made several methodological assumptions. It is hypothesized that the fraction of phosphorylated AMPA receptors can fluctuate significantly within each spine; however, we assume a quantity of AMPARs averaged across a population of synapses. This assumption may be invalid if the total number of AMPARs is small, resulting in fluctuations that are of the same order of magnitude of the mean value. Furthermore, we assume a "well-stirred" system in which all enzymes have equal access to AMPA receptors, which may be invalid if different enzymes are compartmentalized within the synapse. The validity of some of these assumptions was addressed in a recently introduced model based on Monte-Carlo simulations (MCell); however, it remains to be determined whether such issues are fundamental to theoretical modeling of synaptic plasticity (Franks et al. 2002).

We only consider plasticity that is maintained by phosphorylation of the AMPA receptors. Therefore, throughout the model, we assume that the shape of the LTP/LTD curves are equivalent to changes in the conductance of the AMPA receptors. There is strong evidence that additional processes, such as insertion of additional postsynaptic AMPA receptors and/or changes in presynaptic probability of release, are also associated with synaptic regulation (Malinow and Malenka 2002). Such additional mechanisms will modify, but not negate, our results.

The central properties of our model support the postulates of the BCM theory (Bienenstock et al. 1982; Intrator and Cooper 1992; Blais et al. 1999), but our molecular model suggests some modifications. The results depicted here are the steady-state conductance of AMPARs, resulting from a prolonged elevation of intracellular calcium. In a previous study (Shouval et al. 2002b), we obtained a rule for the derivative of the synaptic weight, which seems similar to BCM, but depends on calcium rather then on pre- and postsynaptic activity. We have previously translated our biophysical model into a function of pre- and postsynaptic activity (Castellani et al. 2001; Shouval et al. 2002b); however, we find that unlike BCM, our plasticity equations are no longer linear in presynaptic activity. These differences from the BCM theory are currently under investigation (Yeung et al. 2004). We have recently studied the dynamics of these equations, and have approximated the dynamics of AMPARs' conductance by a simpler dynamical equation that depends directly on calcium (Shouval et al. 2002b). We have also used this equation, which we call the "calcium control hypothesis", as the basis for a unified model of synaptic plasticity. We have shown that this unified model can account for various induction paradigms of synaptic plasticity, including rate-based and spike timing-based protocols (Shouval et al. 2002a). In addition, we have also shown that changes in the properties of NMDAR conductance have the effect of changing the form of the LTP/LTD curves (Castellani et al. 2001; Shouval et al. 2002a,b). Thus, activity-dependent plasticity of NMDAR, which has been observed experimentally (Carmignoto and Vicini 1992; Quinlan et al. 1999; Watt et al. 2000), can serve as a mechanism for metaplasticity (Bienenstock et al. 1982; Abraham and Bear 1996).

Acknowledgments

This research was supported by The Charles A. Dana Foundation and the "Brown University Institute for Brain and Neural Systems," G.C.C. was supported by an exchange program between Bologna and Brown University and MIUR(ex 60%) and FIRB and INFN FB11, and E.M.Q. was supported by the National Institute of Health EY13818. We also thank Dr. Mark Bear and Dr. Hey-Kyoung Lee for useful discussions.

Appendix

Derivation of the calcium-dependent "Flux"

In this section, we derive the calcium-dependent flux for the kinase-1 (K1). We report only one case, because all of the other cases can be obtained following the same procedure.

The relations (equation 14) lead to the following expressions:

$$K1Ca = \frac{K1 \cdot Ca}{k_{E_0}}; \qquad K1 = \frac{k_{E_0} k_{E_1} k_{E_2} k_{E_3} \cdot K1Ca_4}{Ca^4};$$

$$K1Ca_2 = \frac{K1Ca \cdot Ca}{k_{E_1}}; \qquad K1Ca = \frac{k_{E_1} k_{E_2} k_{E_3} \cdot K1Ca_4}{Ca^3};$$

$$K1Ca_3 = \frac{K1Ca_2 \cdot Ca}{k_{E_2}}; \qquad K1Ca_2 = \frac{k_{E_2} k_{E_3} \cdot K1Ca_4}{Ca^2};$$

$$K1Ca_4 = \frac{K1Ca_3 \cdot Ca}{k_{E_3}}; \qquad K1Ca_3 = \frac{k_{E_3} \cdot K1Ca_4}{Ca}.$$

where $K_{E_s} = K_{A_s}/K_{D_s}$. The phosphorylation reactions catalyzed by the fully activated enzyme $K1Ca_4$ are, as usual:

$$K1Ca_4 + A \underset{k_b^1}{\overset{k_f^1}{\rightleftarrows}} K1Ca_4A \overset{k_{irr}^1}{\rightarrow} K1Ca_4 + A_{\mathrm{p1}}$$

$$K1Ca_4 + A^{\mathrm{p2}} \underset{k_b^7}{\overset{k_f^7}{\rightleftarrows}} K1Ca_4A^{\mathrm{p2}} \overset{k_{irr}^1}{\rightarrow} K1Ca_4 + A_{\mathrm{p1}}^{\mathrm{p2}}.$$

These reactions, those for the calcium activation of K1, and the enzyme conservation condition give:

$$K1 + K1Ca + K1Ca_2 + K1Ca_3 + K1Ca_4 + K1Ca_4A + K1Ca_4A^{\mathrm{p2}} = K1_T.$$

By substitution we obtain:

$$K1Ca_4 = (K1_T - K1Ca_4A - K1Ca_4A^{\mathrm{p2}}) \cdot \sigma(Ca)$$

$$\sigma(Ca) = \frac{Ca^4}{k_{E_0}k_{E_1}k_{E_2}k_{E_3} + k_{E_1}k_{E_2}k_{E_3}Ca + k_{E_2}k_{E_3}Ca^2 + k_{E_3}Ca^3 + Ca^4}$$

where σ (*Ca*) is a sigmoidal (Hill) function that expresses the degree of binding of *Ca* with K1.

The steady-state hypothesis for the above reactions give us the following equations:

$$\begin{cases} K1Ca_4 \cdot A - k_{m1} \cdot K1Ca_4A = 0 \\ K1Ca_4 \cdot A^{\mathrm{p2}} - k_{m7} \cdot K1Ca_4A^{\mathrm{p2}} = 0 \end{cases}$$

After substitution for $K1Ca_4$, we obtain a linear system in the unknown $K1Ca_4A$, $K1Ca_4A^{\mathrm{p2}}$:

$$\begin{cases} (\sigma(Ca) \cdot A + k_{m1}) \cdot K1Ca_4A + \sigma(Ca) \cdot A \cdot K1Ca_4A^{\mathrm{p2}} \\ = K1_T\sigma(Ca) \cdot A \\ \sigma(Ca) \cdot A^{\mathrm{p2}} \cdot K1Ca_4A + (\sigma(Ca) \cdot A + k_{m7}) \cdot K1Ca_4A^{\mathrm{p2}} \\ = K1_T\sigma(Ca) \cdot A^{\mathrm{p2}} \end{cases}$$

whose solutions:

$$K1Ca_4A = \frac{K1_T \cdot k_m^7 \cdot \sigma(Ca) \cdot A}{k_m^1k_m^7 + k_m^1 \cdot \sigma_{\mathrm{K1}}(Ca)A^{\mathrm{p2}} + k_m^7 \cdot \sigma_{\mathrm{K1}}(Ca)A}$$

$$K1Ca_4A^{\mathrm{p2}} = \frac{K1_T \cdot k_m^1 \cdot \sigma(Ca) \cdot A^{\mathrm{p2}}}{k_m^1k_m^7 + k_m^1 \cdot \sigma_{\mathrm{K1}}(Ca)A^{\mathrm{p2}} + k_m^7 \cdot \sigma_{\mathrm{K1}}(Ca)A}$$

allow us to define the "Calcium-dependent flux" associated with the kinase K1:

$$\mathscr{F}_{\mathrm{K1}}^{Ca} = \frac{K1_T \cdot \sigma_{\mathrm{K1}}\,(Ca)}{k_m^1k_m^7 + k_m^1 \cdot \sigma_{\mathrm{K1}}(Ca)A^{\mathrm{p2}} + k_m^7 \cdot \sigma_{\mathrm{K1}}(Ca)A}.$$

The same procedure, if applied to the other enzymes, gives us the other "fluxes" that are necessary to write the matrix $\mathscr{P}$ (equation 15). We observe that this procedure also holds if we change the number of enzymes so that we can obtain the expression used in the case where there is only one nonspecific phosphatase.

References

Abraham, W.C. and Bear, M.F. 1996. Metaplasticity: The plasticity of synaptic plasticity. *Trends Neurosci.* **19:** 126–130.

Artola, A. and Singer, W. 1993. Long term depression of excitatory synaptic transmission and its relationship to long term potentiation. *Trends Neurosci.* **16:** 480–487.

Banke, T.G., Bowie, D., Lee, H., Huganir, R.L., Schousboe, A., and Traynelis, S.F. 2000. Control of GluR1 AMPA receptor function by cAMP-Dependent protein kinase. *J. Neurosci.* **20:** 89–102.

Barria, A., Muller, D., Derkach, V., and Soderling, T.R. 1997. Regulatory phosphorilation of AMPA-type glutamate receptors by CaM-KII during long term potentiation. *Science* **276:** 2042–2045.

Bear, M.F., Cooper, L.N., and Ebner, F.F. 1987. A physiological basis for a theory of synapse modification. *Science* **237:** 42–48.

Benke, T.A., Luthi, A., Issac, J., and Collingridge, G. 1998. Modulation of AMPA receptor unitary conductance by synaptic activity. *Nature* **393:** 793–797.

Bienenstock, E.L., Cooper, L.N., and Munro, P.W. 1982. Theory for the development of neuron selectivity: Orientation specificity and binocular interaction in visual cortex. *J. Neurosci.* **2:** 32–48.

Blais, B., Shouval, H., and Cooper, L.N. 1999. The role of presynaptic activity in monocular deprivation: Comparison of homosynaptic and heterosynaptic mechanisms. *Proc. Natl. Acad. Sci.* **96:** 1083–1087.

Brocher, S., Artola, A., and Singer, W. 1992. Intracellular injection of Ca^{2+} chelators blocks induction of long-term depression in rat visual cortex. *Proc. Natl. Acad. Sci.* **89:** 123–127.

Carmignoto, G. and Vicini, S. 1992. Activity dependent increase in NMDA receptor responses during development of visual cortex. *Science* **258:** 1007–1011.

Castellani, G.C., Quinlan, E.M., Cooper, L.N., and Shouval, H.Z. 2001. A biophysical model of bidirectional synaptic plasticity: Dependence on AMPA and NMDA receptors. *Proc. Natl. Acad. Sci.* **98:** 12772–12777.

Cummings, J., Mulkey, R., Nicoll, R., and Malenka, R. 1996. Ca^{2+} signaling requirements for long-term depression in the hippocampus. *Neuron* **16:** 825–833.

Derkach, V., Barria, A., and Soderling, T. 1999. Ca^{2+}/calmodulin-kinase II enhances channel conductance of α-amino-3-hydroxy-5-methyl-4-isoxazolepropionate type glutamate receptors. *Proc. Natl. Acad. Sci.* **96:** 3269–3274.

Dudek, S.M. and Bear, M.F. 1992. Homosynaptic long-term depression in area CA1 of hippocampus and the effects on NMDA receptor blockade. *Proc. Natl. Acad. Sci.* **89:** 4363–4367.

Franks, K.M. and Sejnowski, T.J. 2002. A Monte Carlo model reveals independent signaling at central glutamatergic synapses. *Biophys. J.* **83:** 2333–2348.

Gu, C. and Cooper, D.M.F. 2000. Ca^{2+}, Sr^{2+}, and Ba^{2+} identify distinct regulatory sites on adenylyl cyclase (AC) types VI and VIII and consolidate the apposition of capacitative cation entry channels and Ca^{2+}-sensitive ACs. *J. Biol. Chem.* **275:** 6980–6986.

Huang, L.J. and Taylor, S.S. 1998. Dissecting cAMP binding domain a in the r_αi subunit of cAMP-dependent protein kinase. *J. Biol. Chem.* **273:** 26739–26746.

Intrator, N. and Cooper, L.N. 1992. Objective function formulation of the BCM theory of visual cortical plasticity: Statistical connections, stability conditions. *Neural Networks* **5:** 3–17.

Kameyama, K., Lee, H.-K., Bear, M., and Huganir, R.L. 1998. Involvement of a postsynaptic protein kinase a substrate in the expression of homosynaptic long-term depression. *Neuron* **21:** 1163–1175.

Klee, C.B. and Cohen, G. 1988. *Calmodulin*. Elsevier, Amsterdam.

Lee, H.-K., Kameyama, K., Huganir, R., and Bear, M. 1998. NMDA induces long-term synaptic depression and dephosphorylation of the GluR1 subunit of AMPA receptors in hippocampus. *Neuron* **21:** 1151–1162.

Lee, A.B., Blais, B., Shouval, H.Z., and Cooper, L.N. 2000a. Statistics of lateral geniculate nucleus (lg) activity determine the segregation of on/off subfields for simple cells in visual cortex. *Proc. Natl. Acad. Sci.* **97:** 12875–12879.

Lee, H.-K., Barbarosie, M., Kameyama, K., Bear, M.F., and Huganir, R.L. 2000b. Regulation of distinct AMPA receptor phosphorilation sites during bidirectional synaptic plasticity. *Nature* **405:** 955–959.

Lisman, J.A. 1989. A mechanism for the Hebb and the anti-Hebb processes underlying learning and memory. *Proc. Natl. Acad. Sci.* **86:** 9574–9578.

Lynch, G., Larson, J., Kelso, S., Barrinuevo, G., and Schottler, F. 1983. Intracellular injections of EGTA block induction of hippocampal long-term potentiation. *Nature* **305:** 719–721.

Malinow, R. and Malenka, R. 2002. AMPA receptor trafficking and synaptic plasticity. *Annu. Rev. Neurosci.* **25:** 103–126.

Meyer, T., Hanson, P.I., Stryer, L., and Shulman, H. 1992. Calmodulin trapping by calcium-calmodulin dependent protein kinase. *Science* **256:** 1199–1201.

Mulkey, R. and Malenka, R.C. 1992. Mechanisms underlying induction of homosynaptic long-term depression in area CA1 of the hippocampus. *Neuron* **9:** 967–975.

Mulkey, R.M., Herron, C.E., and Malenka, R.C. 1993. An essential role for protein phosphatases in hippocampal long-term depression.

Science **261:** 1051–1055.
Mulkey, R.M., Endo, S., Shenolikar, S., and Malenka, R. 1994. Involvement of a calcinurin/inhibitor-1 phosphatase cascade in hippocampal long-term depression. *Nature* **369:** 486–488.
Otmakhov, N., Griffith, L.C., and Lisman, J.E. 1997. Postsynaptic inhibitors of calcium/calmodulin-dependent protein kinase type II block induction but not maintenance of pairing-induced long-term potentiation. *J. Neurosci.* **17:** 5357–5365.
Persechini, A. and Cronk, B. 1999. The relationship between the free concentrations of Ca^{2+} and Ca^{2+}-calmodulin in intact cells. *J. Biol. Chem.* **274:** 6827–6830.
Petralia, R.S. and Wenthold, R.J. 1992. Light and electron immunocytochemical localization of AMPA-selective glutamate receptors in the rat brain. *J. Comp. Neurol.* **318:** 329–354.
Quinlan, E.M., Philpot, B., Huganir, R., and Bear, M. 1999. Rapid, experience-dependent expression of synaptic NMDA receptors in visual cortex in vivo. *Nat. Neurosci.* **2:** 352–357.
Roche, K.W., O'Brien, R., Mammen, A., Bernhardt, J., and Huganir, R. 1996. Characterization of multiple phosphorylation sites on the AMPA receptor GluR1 subunit. *Neuron* **16:** 1179–1188.
Segel, I.H. 1975. *Enzyme kinetics-behavior and analysis of rapid equilibrium and steady state enzyme systems*. Wiley, New York.
Shouval, H.Z., Bear, M.F., and Cooper, L.N. 2002a. A unified theory of NMDA receptor-dependent bidirectional synaptic plasticity. *Proc. Natl. Acad. Sci.* **99:** 10831–10836.
Shouval, H.Z., Castellani, G.C., Blais, B.S., Yeung, L., and Cooper, L.N. 2002b. Converging evidence for a simplified biophysical model of synaptic plasticity. *Bio. Cyb.* **87:** 383–391.
Stemmer, P.M. and Klee, C.B. 1994. Dual calcium ion regulation of calcineurin by calmodulin and calcineurin b. *Biochemistry* **33:** 6859–6866.
Walaas, S.I. and Greengard, P. 1991. Protein phosphorylation and neuronal function. *Pharmacol. Rev.* **43:** 299–349.
Wang, J.-H. and Kelly, P.T. 1997. Postsynaptic calcineurin activity downregulates synaptic transmission by weakening intracellular Ca^{2+} signaling mechanisms in hippocampal CA1 neurons. *J. Neurosci.* **17:** 4600–4611.
Watt, A.J., Rossum, M.V., MacLeod, K.M., Nelson, S.B., and Turrogiano, G.G. 2000. Activity coregulates quantal AMPA and NMDA currents at neocortical synapses. *Neuron* **26:** 659–670.
Wenthold, R., Petralia, R., Blahos, J.I., and Niedzielski, A. 1996. Evidence for multiple AMPA receptor complexes in hippocampal CA1/CA2 neurons. *J. Neurosci.* **16:** 1982–1989.
Yeung, L.C., Shouval, H.Z., Blais, B.S., and Cooper L.N. 2004. Homeostasis and pattern formation under a NMDAR-mediated, calcium-dependent synaptic plasticity model. *Proc. Natl. Acad. Sci.* **101:** 14943–14948.

Received April 27, 2004; accepted in revised form May 17, 2005.